Egypt. J. Chem. Vol. 67, SI: M. R. Mahran, pp. **1333 - 1345** (2024)

Egyptian Journal of Chemistry

http://ejchem.journals.ekb.eg/

Study of Tertralone Derivatives as Potent Anti-Cancer Agents through Apoptosis assessment: In Vitro and In silico Approaches

Marwa M. Mounier[1], Hanaa S. Mohamed [2] , Ahmed A. El-Rashedy[*3]

1Department of Pharmacognosy, Pharmaceutical and Drug Industries Research Institute, National Research Centre, Dokki, Egypt

2Department of Therapeutic Chemistry, Pharmaceutical and Drug Industries Research Division, National Research Center, El Buhouth Street, Dokki, Cairo, 12622, Egypt

3Chemistry of Natural and Microbial Products Department, National Research Center, 33 elBehouth St., Dokki, Giza, Egypt.

Abstract

Tetralone derivatives have previously proven their potential activity as anticancer candidates. The potential anticancer activity of a series of tetralone compounds 3–14 with a sulfonamide scaffold was synthesized and investigated.. The invitro anticancer evaluation in the present study was done on a seven different human cancerous cells. Following studying the safety of all the synthesized compounds on normal human cells, IC_{50} values were identified for promising compound **14**. Our findings showed that compound 11 selectively has anti-breast potentiality (MCF-7). Upon studying the molecular effect of compound 11 on different apoptotic proteins like BCL2, Bax, and caspase-7, compound 11 signaled an apoptotic cascade in breast cancer cells, producing cell cycle arrest at the G2/M phase. Investigation of the binding interaction, dynamic nature, and protein-ligand stability was carried out using molecular dynamics (MD) simulation. MD simulation analytical characteristics (RMSD, RMSF, and RoG) indicated that compound **11** was stable during the 20 ns MD simulation investigation. Meanwhile, MD simulation showed that compound **11** selectively targeted the catalytic-binding pocket residues, with the naphthalene group interacting into the small hydrophobic pocket provided by Asn 94, Arg 133, Tyr 137, Ile 139, Ala 148, Tyr 149, Cys 196, Val 197, and Val 198 in caspase-7, and by the residues Tyr 46, Ala 49, Phe 50, Leu 53, Val 71, Leu 75, Arg 84, Ala 87 and Ser 90 in BCL2 receptor. The absorption, metabolism, and carcinogenic properties of compound **11** ADMET predictions were carried out. Based on our physicochemical, docking, dynamics simulation, and ADMET prediction results, compound 11 is considered as a new effective and selective anticancer candidate.

.

Keywords: Tetralone, Anti-Cancer, Apoptosis

1. Introduction

Cancer is one of humanity's greatest issues due to its tremendous impact on human health and the economy (1,2) . Based on GLOBOCAN's estimates, around the world, there were approximately 19.3million new cancer cases and 10.0million deaths in 2020 worldwide (3). Early on, Conventional cancer chemotherapy is primarily inadequate due to the lack of selectivity of a large majority of drugs for targeting cancer cells over their non-cancerous counterparts (4). Cytotoxic compounds were used to treat cancer, but there was a high risk due to the possibility of causing damage to normal and healthy cells. However, the development of new classes of anticancer agents with both effective and selective toxicity towards cancer cells is attracting great interest due to the unwanted side effects of many chemotherapy drugs.

Apoptosis, a controlled sort of intentional cell death, is required for multicellular creatures to develop properly. In cancer, apoptosis mechanisms are typically dysregulated. The creation of specialized drugs to reactivate the apoptotic process is a sound strategy. The intrinsic and extrinsic pathways are the two main pathways of apoptosis.

Caspase-7 is a caspase (cysteine aspartate protease) family protein that has been identified to serve a key function in the execution phase of cell apoptosis.

Intrinsic apoptosis is defined by a change in mitochondrial outer membrane permeabilization (MOMP), which is tightly regulated by family proteins BCL-2, which are classified into three groups: anti-apoptotic proteins like BCL-2, MCL-1, BCL-XL, BCL-W, and BFL-1/A1, and pre-apoptotic proteins like BAX, BOK and BAK. (5) . BCL-2 protein family

*Corresponding author e-mail Ahmedelrashedy45@gmail.com .; (Ahmed A. Elrashedy).

Receive Date: 11 June 2024, Revise Date: 20 July 2024, Accept Date: 22 July 2024

DOI: 10.21608/EJCHEM.2024.296982.9849

members are dysregulated in many malignancies, therefore targeting them may cause cancer cell death.

Studies revealed that, when tetrahydronaphthalene derivatives (tetralone derivatives) incorporated to or attached with different heterocyclic moieties were evaluated for their *in vitro* anticancer activity, they demonstrated moderate to marginal efficacy against the breast carcinoma cell line MCF-7 (6). In addition, Longifolene-derived tetralone (3,4-dihydronaphthalen-1(2H)-one) compounds, carrying a 1,2,4-triazole heterocycle, demonstrated superior anticancer activity against the present cancer cell lines as compared to the reference drug 5-FU (7).

On the other hand, several sulfonamide compounds (**14)** are used marketed as antineoplastic drugs such as, Belinostat which is a histone deacetylase (HDAC) inhibitor (8) and Pazopanib that acts through tyrosine kinases VEGF and PDGF inhibition (9) .

Furthermore, sulfonamide derivatives of the structure (A) were used to treat proliferative disorders (i.e. preneoplastic and/or neoplastic diseases) by specifically inhibiting the carbonic anhydrase activity of proteins (10).

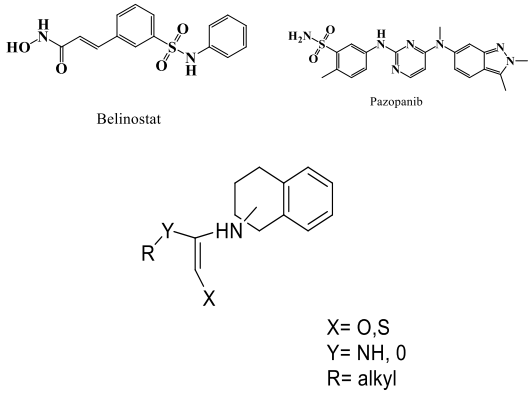

(A)

Based on these findings, compounds with a sulfonamide moiety and a tetrahydronaphthalene scaffold in the same structure have gotten a lot of attention in our research because of their broad chemotherapeutic potential.

In this study, the cytotoxic activity of the synthesized tetrahydro-naphthalene sulfonamide compounds was tested *in vitro* against seven different types of human tumor cell lines: colorectal carcinoma (HCT-116 cell line), breast carcinoma (MCF-7 cell line), prostate cancer (PC3 cell line), lung carcinoma (A-549 cell line), melanoma (A-375 cell line), colon cancer (caco2 cell line), liver carcinoma (HepG2), and towards the human normal cells (BJ-1). Furthermore, a molecular dynamic research was carried out to estimate the inhibitory mode of action of the most active compound.

2. Results and discussion

2.1. Chemistry

Tetrahydronaphthalene- sulfonamide derivatives **3-14** scheme 1 were synthesized according to our previously published paper (11). However, the key intermediate was 3–methoxy-8-oxo- 5,6,7,8-tetrahydronaphthalene-2-sulfonyl chloride **2** was obtained from the reaction 6–methoxy-1-tetralone **1** with sulfurochloridic acid and thionyl chloride in a good yield, where compound **2** underwent simple coupling with primary or secondary amines (ethylamine, 4-chloroaniline, 4-fluroaniline, 4-aminobenzoic acid, p-anisidine, valine, 2-aminouracile, 2-aminobenzimidazole, piperidine, morpholine, methyl piperazine) to give the corresponding tetrahydronaphthalene- sulfonamide derivatives

3-13.

On the other hand, treatment of the chlorosufonyl compound 2 with excess hydrazine hydrate lead to the formation of 8-hydrazineylidene-3–methoxy-5,6,7,8-tetrahydronaphthalene-2-sulfonohydrazide **14**. All the prepared compounds were confirmed by the different spectroscopic analysis and were carried to evaluate their cytotoxic activity against different seven cancer cell lines.

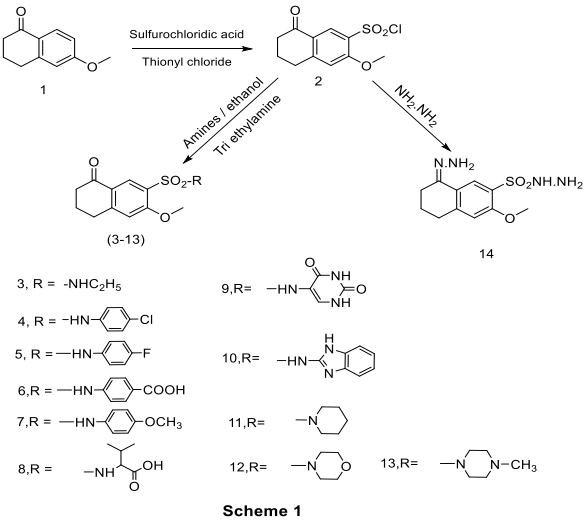

Scheme 1

2.2 Biological part:

2.2.1 In vitro anticancer activity against human cell lines

Twelve chemical compounds were screened for their cytotoxic activity using MTT assay towards seven different human cancer cell lines, at starting concentration of 50 μM, namely, A-375 skin tumor cell line, MCF-7 breast cancer cell line, HCT-116 colon cancer cell line, prostate cancer cell line PC3, lung cancer cell line A-549, colon cancer cell line caco2 and liver cancer cell line HepG2 and Doxorubicin was used as a reference drug as presented in the following **Table 1**.

Table 1: % of growth inhibition of all synthesized compounds towards seven human tumor cell lines (A-375, MCF-7, HCT-116, PC3, A-549, caco2, HepG2) at 50 µM. Every value is an average of three readings

	Growth Inhibition %						
Compound	**A-375**	**MCF-7**	**HCT-116**	**PC3**	**A-549**	**caco2**	**HepG2**
3	2.1±0.2	1.4±0.2	3.5±0.1	22.1±0.3	9.8±0.9	9.8±1.3	8.8±0.3
4	2.3±0.4	8.3±0.8	39.9±0.8	11.2±0.2	30.7±1.8	12.1±0.9	3.7±0.3
5	1.1±0.1	19.4±0.9	4.5±0.2	13.6±1.1	23.5±0.8	16.5±0.3	13.2±0.1
6	0.8±0.3	8.1±1.1	26.7±0.5	9.5±0.3	24.7±0.7	18.5±0.4	17.6±0.6
7	7.9±0.4	8.2±0.9	44.5±0.8	27.9±0.4	33.1±1.1	13.2±0.5	17.3±1.1
8	1.5±0.1	0.7±0.3	11.9±0.2	13.8±1.1	47.5±1.9	14.7±1.1	6.8±0.8
9	1.2±0.2	0.8±0.2	1.7±0.05	14.2±0.4	10.8±0.6	3.2±0.4	10.9±0.2
10	0.9±0.4	2.7±0.4	6±0.9	23.9±1.2	29.8±0.3	8.8±0.4	3.2±0.4
11	20.3±0.8	77.5±1.3	39.1±1.1	5.9±0.7	45.1±0.6	54.4±1.1	48.4±1.1
12	0.5±0.1	2.1±0.5	14.2±0.5	32.5±2.1	25.9±1.1	13.7±0.7	1.6±0.05
13	0.7±0.2	4.7±0.1	9.1±1.1	14.8±0.6	21±2.3	12±0.9	23±0.6
14	0.2±0.05	29.7±0.7	0±0.005	22.8±0.7	9.6±0.8	16±2.1	31.6±0.4
Doxorubicin	99.9±1.4	86.8±1.8	67.8±2.1	84.4±0.9	62.6±1.1	98.9±1.7	89.3±12.1

According to our results, all of the tested compounds showed weak cytotoxic activity < 40% on skin and prostate cancer cell lines A-375 and PC3. While compounds **7, 8**& **11** gave moderate activity > 40% cytotoxic activity on HCT-116, A-549, caco2, and HepG2 respectively. On the contrary, compound **11** showed potent significant activity on human cancer breast cells MCF-7 with 77.5% of growth inhibition. Moreover, all compounds under study were subjected to screen their specificity towards the normal cells BJ-1. According to our results, all synthesized compounds possessed significant safety with weak cytotoxic activity ranging from 0.1- 34.3 growth inhibition (GI) % on the normal cell line (BJ-1) with better safety response than reference drug doxorubicin Figure 1. Based on the current finding, compound **11** showed selective potent anti-breast cancer activity which encourages us to further elucidate their apoptotic effect on different apoptotic proteins.

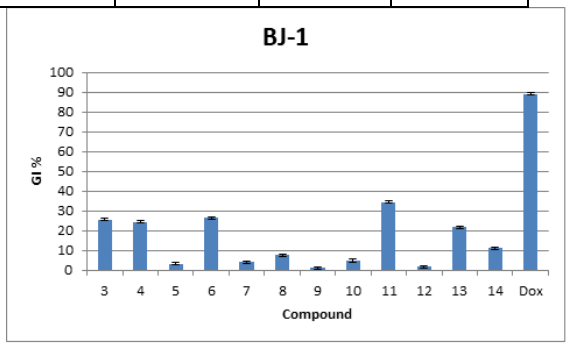

Figure 1: Growth inhibition % of all synthesized compounds against normal cells (BJ-1) at 50 µM, Values shown are mean ± S.D. (n = 3).

2.2.2 Cellular mode of action

2.2.2.1 Cell apoptosis.

Effect of compound **11** on the level of BCL2, BAX, BAX/BCL2 ratio and caspase-7 in MCF-7

Compound **11** was further screened in dose dependent manner on MCF-7 to determine their IC_{50} value, 35.6 µM,. Then MCF-7 was treated with IC_{50} of compound **11** for 24hr, and BAX, BCL2, and caspase 7 proteins were estimated. Compound **11** manage to upregulate apoptotic protein Bax from 41.7 to 203.6 Pg/ml and downregulate antiapoptotic protein BCL2 from 8.25 to 5.68 ng/ml compared to untreated MCF-7 cells. Compound **11** also signal caspase 7 inside MCF-7 treated cells from 0.5 to 2.2 ng/ml as shown in **Figure 2**.

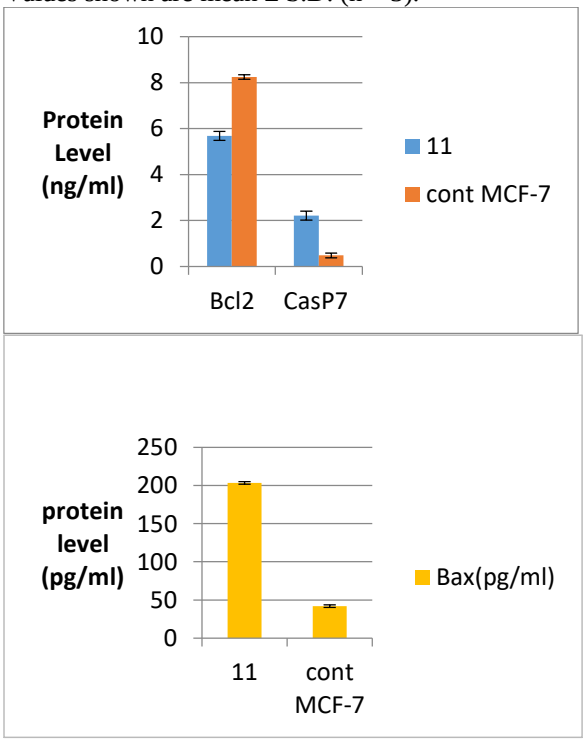

Figure 2: BCL2, caspase-7, BAX protein level of untreated MCF-7 (cont) and treated one with compound **11** for 24 hr.

2.2.2.2 Cell cycle arrest.

To confirm the apoptotic effect of compound **11**, cell cycle analyses were done. Compound **11** signal early apoptosis and late apoptosis from 0.43-2.84 & 0.15-10.27 respectively. These results are following our results and confirm the apoptotic effect of compound **11**. Treated MCF-7 with IC_{50} of compound **11** resulted in an increase in cell percentage G2/M phase from 8.36 to 15.9 leading to cell accumulation at Pre-G1, 11.7 fold from 1.63 to 19.08 as compared to untreated MCF-7 cells as a result of cell cycle arrest@G2/M phase.

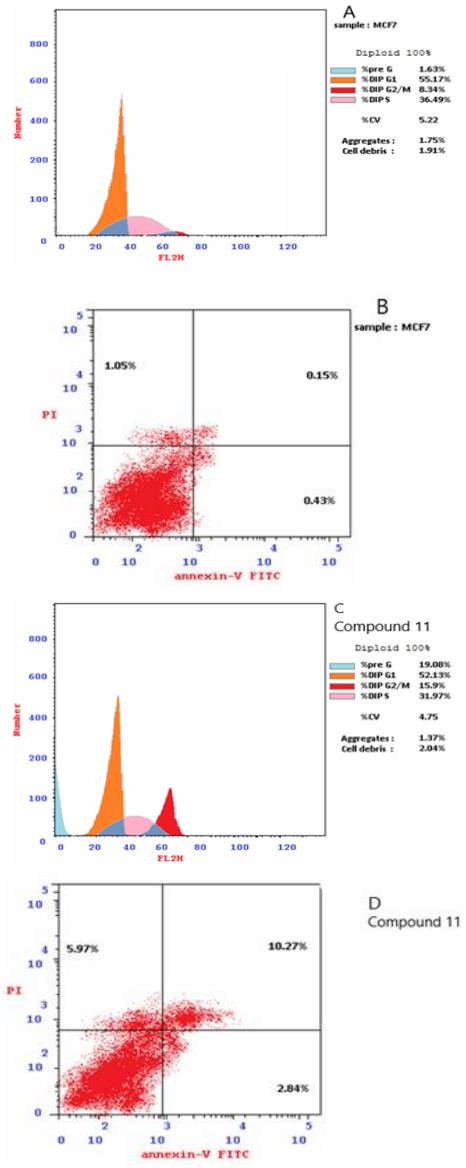

Figure 3. Cellular mechanism of action of untreated MCF-7 (A, B). MCF-7 was treated with compound **11** for 24 h and analyzed by annexin V/PI staining. The apoptotic cells percentage is the sum of early apoptotic (annexin V+/PI−) cell percentage and late apoptotic (annexin V+/PI+) cell percentage. (C, D) Cell cycle analysis of MCF-7 incubated with compound for 24 hr.

2.3. Molecular dynamic study

2.3.1. Molecular dynamic and system stability :

The effectiveness of the tested compound when it binds to the protein's active site as well as its interaction and stability were predicted using a molecular dynamic simulation (12,13). To track down disturbed motions and keep simulation artefacts at bay, the system's stability must be validated. The stability of the systems was measured in this study using the Root-Mean-Square Deviation (RMSD) during the 20 ns simulations. The stability of the systems was measured in this study using the Root-Mean-Square Deviation (RMSD) during the 20 ns simulations. Figure 4A shows that the average RMSD values for the apo-protein system across all frames and the 11-complex system for Capases 7 were 1.36± 0.23 Å and 1.20 ±0.10 Å, respectively. While Bcl2's average RMSD values were 1.55± 0.23 Å and 1.50 ±0.19 Å for all frames of the apo-protein and 11-complex systems, respectively. Figure 5a. These findings showed that, compared to the other investigated system, the complex system of protein 11 had acquired a considerably more stable conformation. Examining residue behaviour and its relationship with the ligand during MD simulation requires evaluating protein structural flexibility upon ligand binding(13). Using the Root-Mean-Square Fluctuation (RMSF) technique, protein residue variations were assessed to determine the impact of inhibitor binding to the relevant targets across 20 ns of simulations. For the apo-protein and 11-complex systems, the calculated average RMSF values for capase -7 were 4.8746± 0.09 Å and 1.03 ±0.60 Å, respectively, Figure 4B. Figure 5b shows that the average RMSF values for BCL2 were 6.86 Å for apo-protein and 0.97 Å for the 11-complex system, respectively. In Figure 4B,5b, the overall residue fluctuations of several systems are depicted. These numbers demonstrated that the complex system of protein 11 had a lower residue fluctuation than the other system.

The protein structural compactness and simulation stability are both indicated by the radius of gyration (Rg). As seen in Figure 4C, the Rg values of the apo-protein and complex with compound 11 were 16.75± 0.07 Å and 16.16 ±0.06 Å for the capase -7 receptor, respectively, whereas the values were 16.68± 0.14 Å and 16.61± 0.09 Å for the BCL2 receptor. Rg of ligand-bonded proteins was discovered to have a less rigid structure than Apo-protein.

2.3.2. Binding interaction mechanism based on binding free energy calculation:

A well-known technique for determining the free binding energies of small compounds to biological macromolecules is the molecular mechanics energy methodology (MM/GBSA), which combines generalised Born and surface area continuum solvation(14). It may be more accurate than docking scores.

The MM-GBSA tool in AMBER18 was used to determine the binding free energies by taking snapshots of the systems' trajectories. All of the estimated energy components presented (apart from Gsolv), as seen in Table 1, had substantial negative values, indicating positive interactions.BCL2 and 11-bonded to Capase protein had binding affinities of -22.36 kcal/mol and -36.16 kcal/mol, respectively, according to Table 2.

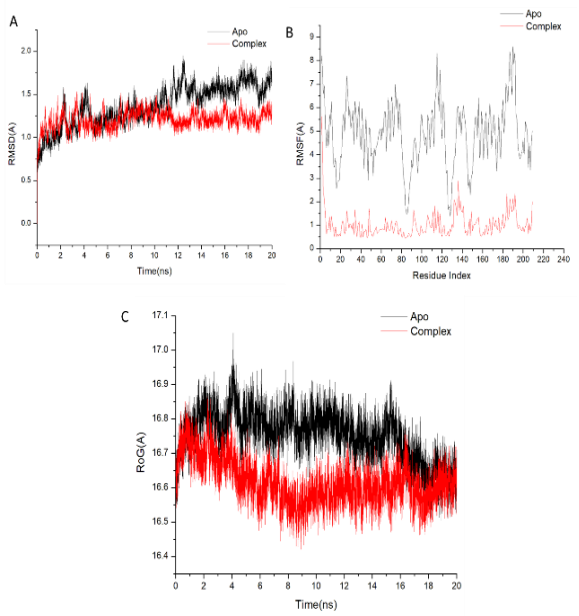

Figure 4: [A] RMSD of Cα atoms of the protein backbone atoms. [B] RMSF of each residue of the protein backbone Cα atoms [C] RoG of Cα atoms of protein residues of the backbone atoms relative (black) to the starting minimized over 20 ns for the caspase-7 protein with ligand 11(red).

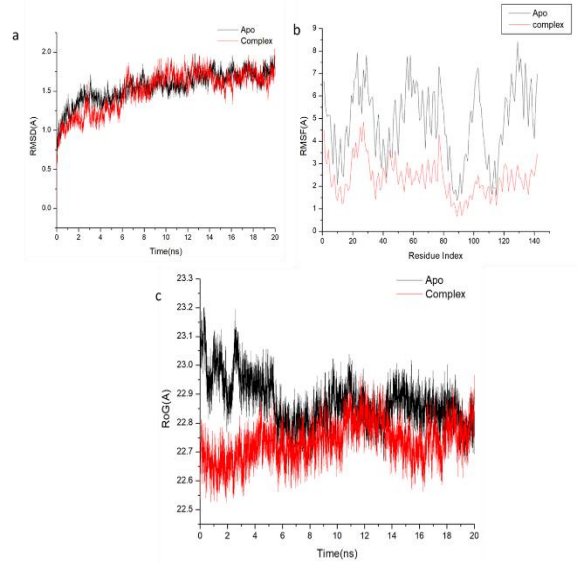

Figure 5: [a] RMSD of Cα atoms of the protein backbone atoms. [b] RMSF of each residue of the protein backbone Cα atoms [c] ROG of Cα atoms of protein residues of the backbone atoms relative (black) to the starting minimized over 20 ns for the BCL-2 protein with ligand **11**(red).

Table 2: Shows the calculated energy binding for the compound **11** against the caspase-7 , and BCL2 receptors .

Energy Components (kcal/mol)					
Complex	**ΔE_{vdW}**	**ΔE_{elec}**	**ΔG_{gas}**	**ΔG_{solv}**	**ΔG_{bind}**
11-Caspase	-33.35± 0.22	-18.92± 0.32	-52.27± 0.37	16.11± 0.30	-36.16± 0.27
11-BCL2	-27.77± 0.22	-2.96± 0.44	-28.73± 0.47	6.36± 0.35	-22.36± 0.25

ΔEvdW = van der Waals energy; ΔEele = electrostatic energy; ΔGsolv = solvation free energy; ΔGbind = calculated total binding free energy.

A thorough examination of each individual energy contribution, leading to the reported binding free energies, revealed that the interactions between caspase-7 receptor, BCL2 protein receptor residues, and compound **11** were driven by the higher positive vander Waals energy components Table 1.

2.3.3. Identification of the critical residues responsible for ligands binding:

The overall energy involved when 11 binds these enzymes was further broken down into the involvement of specific site residues in order to better understand the important residues involved in suppressing the caspase-7 receptor protein receptor. From Figure. 6, the major favorable contribution of **11** compound to the caspase-7 protein receptor is predominantly observed from residues Asn 94 (-0.334 kcal/mol) , Ile 105 (-0.182 kcal/mol), Ile 129 (-0.103 kcal/mol), Arg 133 (-1.503 kcal/mol), Tyr 137 (-2.309 kcal/mol), Ile 139 (-0.788 kcal/mol), Leu 146 (-0.239 kcal/mol), Phe 147 (-0.397 kcal/mol), Ala 148 (-0.56 kcal/mol), Tyr 149 (-1.432 kcal/mol), Pro 195 (-0.42 kcal/mol), Cys 196 (-1.974 kcal/mol), Val 197 (-0.716 kcal/mol), and Val 198 (-1.152 kcal/mol. On the other hand , the major favorable contribution of compound **11** to the BCL-2 protein receptor is predominantly observed from residues Phe 42 (-0.339 kcal/mol) , Tyr 46 (-0.91 kcal/mol), Ala 49 (-0.443 kcal/mol), Phe 50 (-0.905 kcal/mol), Leu 53 (-1.103 kcal/mol), Val 71 (-0.576 kcal/mol), Glu 74 (-0.407 kcal/mol), Leu 75 (-2.159 kcal/mol), Arg 77 (-0.278 kcal/mol), Arg 84 (-2.088 kcal/mol), Val 86 (-0.202 kcal/mol), Ala 87 (-0.699 kcal/mol), and Ser90 (-0.152 kcal/mol).

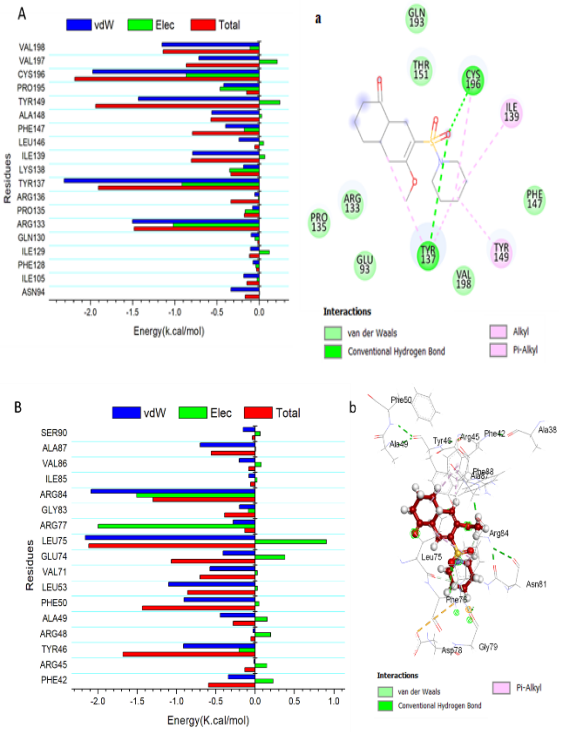

Figure 6*: Per-residue decomposition plots showing the energy contributions to the binding and stabilization of compound* ***11*** *at the catalyatic active site of the caspase-7 receptor [A],BCL2 receptor [B] . Corresponding inter-molecular interaction of compound* ***11*** *to the the catalyatic active site of the caspase-7 receptor [a], BCL2 receptor [b] .*

2.3.4. ADMET prediction

Because of inadequate ADMET qualities, many drug molecule candidates stay in phase investigations without a drug molecule. Advanced in vitro and in vivo research on the chemical may benefit from performing some theoretical ADMET calculations on freshly discovered and synthesised molecules. Numerous properties of the created compounds, including physiochemical, lipophilicity, water solubility, and pharmacokinetics, are the result.

The medicinal chemical properties and drug-likeness of molecule 11 were estimated using SwissADME online tools, and some of its most potent characteristics are shown in Table 3. Each feature falls within the acceptable range (15), including XLOGP3 = 4.25 (-0.7 to + 5.0), Molecular weight = 325.42 g/mol (150 to 500 g/mol), Solubility (Log S) = -2.58 (log S not larger than 6), and Flexibility (FLEX) = 3 (no more than 9 rotatable bonds).It is not very soluble in water.It was shown to have a high rate of absorption through the gastrointestinal tract and to be unable to penetrate the blood–brain barrier.It does not interact with other medications because it does not affect Cyp enzymes. While druglikeness is high according to Ghose and Egan, it is appropriate according to Lipinski, Veber, and Muegge's rigorous standards. The lead resemblance characteristic deviates from the shortening rules in two ways. Other medicinal chemistry criteria can be used.

Table 3 : Physiochemical, lipophilicity, water-solubility, pharmacokinetics, druglikeness, and medicinal chemistry properties of compound 11.

Physicochemical Properties	
Formula	C16H23NO4S
Molecular weight	325.42 g/mol
Num. heavy atoms	22
Num. arom. heavy atoms	0
Fraction Csp3	0.69
Num. rotatable bonds	3
Num. H-bond acceptors	5
Num. H-bond donors	0
Molar Refractivity	88.80
TPSA	72.06 Å²
Lipophilicity	
Log Po/w (iLOGP)	2.16
Log Po/w (XLOGP3)	1.46
Log Po/w (WLOGP)	2.92
Log Po/w (MLOGP)	0.86
Log Po/w (SILICOS-IT)	1.22
Consensus Log Po/w	1.72
Water Solubility	
Log S (ESOL)	-2.58
Solubility	8.57e-01 mg/ml ; 2.63e-03 mol/l
Class	Soluble
Log S (Ali)	-2.58
Solubility	8.57e-01 mg/ml ; 2.63e-03 mol/l
Class	Soluble
Log S (SILICOS-IT)	-2.34
Solubility	1.49e+00 mg/ml ; 4.58e-03 mol/l
Class	Soluble
Pharmacokinetics	
GI absorption	High
BBB permeant	Yes
P-gp substrate	No
CYP1A2 inhibitor	No
CYP2C19 inhibitor	No
CYP2C9 inhibitor	No
CYP2D6 inhibitor	No
CYP3A4 inhibitor	No
Log Kp (skin permeation)	-7.25 cm/s
Druglikeness	
Lipinski	Yes; 0 violation
Ghose	Yes
Veber	Yes
Egan	Yes
Muegge	Yes
Bioavailability Score	0.55
Medicinal Chemistry	
PAINS	0 alert
Brenk	0 alert
Leadlikeness	Yes
Synthetic accessibility	4.62
Bioactivity and toxicity risk	
Mutagenic	None
Tumorigenic	None
Reproductive effective	None
Irritant	None
GPCR ligand	-0.13
Ion channel modulator	-0.55
Kinase inhibitor	-0.54
Nuclear receptor ligand	-0.20

Protease inhibitor	0.17
Enzyme inhibitor	0.10
Boiled-Egg' method summary	
Bioavailability radar	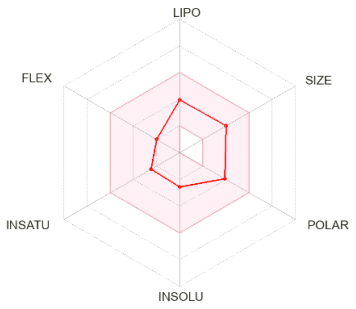
The BOILED-Egg model	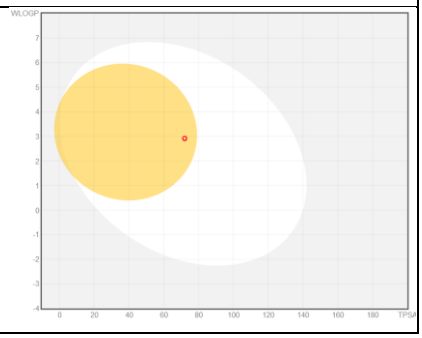

3 -Experimental

3.1 Chemistry

Tetrahydronaphthalene-sulfonamide derivatives **3-14** under investigation were synthesized according to the method described elsewhere(11) The structures of the synthesized compounds were confirmed with the different spectral data (IR, 1H NMR, 13C NMR and Mass spectroscopy).

Synthesis of 3-methoxy-8-oxo-5,6,7,8-tetrahydronaphthalene-2-sulfonyl chloride 2

In ice bath, chlorosulfonic acid (60 mmol) was cooled till zero ºC, followed by dropwise addition of thionyl chloride (20 mmol) while stirring. The mixture was kept under stirring at zero ºC for about 30 min. To the stirred solution, 6-methoxy-1-tetralone **1** (10 mmol) was added portion wise. After complete addition, the reaction mixture was stirred at room temperature for about 24 h., till completion of the reaction, the mixture was poured onto ice cold water, and the formed precipitate was filtered off quickly, washed with cold water. Pure product was collected without any need to be purified to yield compound **2**

General procedure for the synthesis of compounds 3-13

To a mixture of the sulfonyl chloride derivative **2** (0.3 mmol) and the suitable amine (0.3 mmol) in ethanol (5 mL), drops of triethyl amine was added, the reaction mixture was left under stirring at room temperature for about 2h. The solid product was filtered off, washed with dilute ethanol, producing compounds **3-13** respectively and recrystallized from the suitable solvent.

Synthesis of (Z)-8-hydrazineylidene-3-methoxy-5,6,7,8-tetrahydronaphthalene-2-sulfonohydrazide 14

To a mixture of the sulfonyl chloride derivative **2** (0.31 mmol) and hydrazine hydrate (excess) in ethanol (5 mL), drops of triethyl amine was added. The reaction mixture was left under stirring at room temperature for about 2h. After that, the solvent was evaporated. The solid product was filtered off, washed with dilute ethanol and recrystallized producing compound **14**.

3.2 .biology

- Anti-Cancer Activity

- Cell Lines

human colorectal carcinoma (HCT-116 cell line), human breast carcinoma (MCF-7 cell line), human prostate cancer (PC3 cell line), human lung carcinoma (A-549 cell line), human melanoma (A-375 cell line), human colon cancer (caco2 cell line), human liver carcinoma (HepG2), and normal human cell line (BJ-1); "a telomerase immortalized normal foreskin fibroblast cell line" were obtained from Karolinska Center, Department of Oncology and Pathology, Karolinska Institute, Stockholm, Sweden.

- Cell Culture

Culturing and subculturing were carried out according to (16). Doxorubicin was used as a positive control. A negative control, composed of DMSO, was also used.

- Cell Viability Assay

This was done according to (17). The cells were seeded at concentration of 10 *10^3cells per well in case of MCF-7 and PC3 and HepG 2, 20 *10^3 cells/well in case of A-549, HCT-116, caco2, and A-375 cell lines and 35–45 *10^3cells/well in case of BJ-1 using 96-well plates at 37°C. After 48 h of incubation, the medium was aspirated and 40 uL MTT salt (2.5 mg/mL) were added and further incubated for 4 h. Then, 200 uL 10% sodium dodecyl sulphate (SDS) was added. The absorbance was measured at 595 nm.

- Determination of IC_{50} Values

IC_{50} values were calculated, using a probit analysis, and by utilizing the SPSS computer program (SPSS for windows, statistical analysis software package/version 9/1989 SPSS Inc., Chicago, IL, USA).

- Human CASP-7 (Caspase-7), BCl-2, BAX Estimation

The micro ELISA plate provided in this kit is pre-coated with the desired specific antibody to be detected. The procedure of CASP-7, BCL-2, and BAX was done according to (18–20) , respectively. . The optical density (OD) was measured at a wavelength of 450 nm ± 2 nm.

- Cell cycle analysis and apoptosis detection

Cell cycle analysis and apoptosis detection were carried out by flow cytometry. MCF-7 cells were seeded at 1-5×10^4 and incubated at 37 °C, 5% CO2 overnight, After treatment with the tested compound 11, for 24 h, cell pellets were collected and centrifuged (300×g, 5 min). For cell cycle analysis, cell pellets were fixed with 70% ethanol on ice for 15 min and collected again (21).The collected pellets were incubated with propidium iodide (PI) staining solution at room temperature for 1 h. Apoptosis detection was performed by Annexin V-FITC apoptosis detection kit (BioVision, Inc, Milpitas, CA, USA) following the manufacturer's protocol. The samples were analyzed using FACS Calibur flow cytometer (BD Biosciences, San Jose, CA).

3.3 Molecular dynamic study

- System preparation

The crystal structure of both caspase-7 and Bcl-2 were retrieved from the protein data bank with codes 1SHJ (22),and 3SPF (23). . These structures were then prepared for molecular dynamics (MD) studies using UCSF Chimera (24). Using PROPKA, pH was fixed and optimized to 7.5(25). 11 structure was drawn using ChemBioDraw Ultra 12.1(26). Altogether, all two prepared systems were subjected to 20 ns MD simulations as described in the simulation section.

- Molecular dynamic (MD) simulations

The integration of Molecular dynamic (MD) simulations in biological systems' study enable exploring the physical motion of atoms and molecules that cannot be easily accessed by any other means(27) .The insight extracted from performing this simulation provides an intricate perspective into the biological systems' dynamical evolution, such as conformational changes and molecule association (27) .The MD simulations of all systems were performed using the GPU version of the PMEMD engine present in the AMBER 18 package (28).

The partial atomic charge of each compound was calculated with ANTECHAMBER's General Amber Force Field (GAFF) technique (29) . The Leap module of the AMBER 18 package implicitly solvated each system within an orthorhombic box of TIP3P water molecules within 10 Å of any box edge. The Leap module was used to neutralize each system by incorporating Na+ and Cl- counter ions. A 2000-step initial minimization of each system was carried out in the presence of a 500 kcal/mol applied restraint potential, followed by a 1000-step full minimization using the conjugate gradient algorithm without restraints.

During the MD simulation, each system was gradually heated from 0K to 300K over 500ps, ensuring that all systems had the same amount of atoms and volume. The system's solutes were subjected to a 10kcal/mol potential harmonic constraint and a 1ps collision frequency . Following that, each system was heated and equilibrated for 500ps at a constant temperature of 300K.To simulate an isobaric-isothermal (NPT) ensemble, the number of atoms and pressure within each system for each production simulation were kept constant, with the system's pressure maintained at 1 bar using the Berendsen barostat (30).

For 20 ns, each system was MD simulated. The SHAKE method was used to constrain the hydrogen bond atoms in each simulation. Each simulation used a 2fs step size and integrated an SPFP precision model. An isobaric-isothermal ensemble (NPT) with randomised seeding, constant pressure of 1 bar, a pressure-coupling constant of 2ps, a temperature of 300K, and a Langevin thermostat with a collision frequency of 1ps was used in the simulations.

- Post-MD Analysis

After saving the trajectories obtained by MD simulations every 1 ps, the trajectories were analyzed using the AMBER18 suite's CPPTRAJ (31) module. The Origin (32) data analysis program and Chimera (33) were used to create all graphs and visualizations.

- Thermodynamic calculation

The Poisson-Boltzmann or generalized Born and surface area continuum solvation (MM/PBSA and MM/GBSA) approach has been found to be useful in the estimation of ligand-binding affinities(34–36) . The Protein-Ligand complex molecular simulations used by MM/GBSA and MM/PBSA compute rigorous statistical-mechanical binding free energy within a defined force field.

Binding free energy averaged over 500 snapshots extracted from the entire 50 ns trajectory. The estimation of the change in binding free energy (ΔG) for each molecular species (complex, ligand, and receptor) can be represented as follows (37) :

$$\Delta G_{bind} = G_{complex} - G_{receptor} - G_{ligand} \quad (1)$$

$$\Delta G_{bind} = E_{gas} + G_{sol} - TS \quad (2)$$

$$E_{gas} = E_{int} + E_{vdw} + E_{ele} \quad (3)$$

$$G_{sol} = G_{GB} + G_{SA} \quad (4)$$

$$G_{SA} = \gamma SASA \quad (5)$$

The terms Egas, Eint, Eele, and Evdw symbolize the gas-phase energy, internal energy, Coulomb energy, and van der Waals energy. The Egas was directly assessed from the FF14SB force field terms. Solvation-free energy (Gsol) was evaluated from the energy involvement from the polar states (GGB) and non-polar states (G). The non-polar solvation free energy (GSA) was determined from the Solvent Accessible Surface Area (SASA)(38,39) using a water probe radius of 1.4 Å. In contrast, solving the GB equation assessed the polar solvation (GGB) contribution. Items S and T symbolize the total entropy of the solute and temperature, respectively.

- ADME prediction

SwissADME (http://www.swissadme.ch/) was used to estimate the compound's physiochemical, lipophilicity, water-solubility, pharmacokinetics, drug-likeness, and medicinal chemistry properties, and OSIRIS property explorer was used to calculate

toxicity parameters such as mutagenicity, tumorigenicity, irritating effects, and reproductive effects.

4. Conclusion

Herein, among the twelve investigated tetrahydronaphthalene sulfonamide derivatives **3-14** , compound **11** exhibited the most efficient product, with specific selectivity against the human breast cancer cells; MCF-7. The apoptotic protein estimation confirmed the intrinsic apoptotic potentiality by affecting BCL2 proteins and signaling execution caspase 7. Therefore, Compound **11** consider a good anticancer candidate as it manages to cause breast cell cycle arrest at G2/M phase. Following that, the interaction's stability was assessed using a typical atomistic 20 ns dynamic simulation study. A number of parameters derived from MD simulation trajectories were computed and validated for the protein-ligand complex's stability under the dynamic conditions. comparative MD simulation and binding free energy analysis were employed to investigate the selectivity mechanism of compound **11** against caspase-7 and BCL2 receptor .Differential binding of 11 to these protein targets was measured using the MM/GBSA method, which revealed favourable interactions with ΔG values of --36.16kcal/mol (caspase-7) and -22.36kcal/mol (BCL2) .The likeness in binding free energies indicated analogous binding modes and affinity as reported previously. The binding free energy component analysis suggests that the major energy component driving this synergistic effect is van der Waals energy component. . The decomposition of the total energies into caspase-7 and BCL2 receptor active site residue contributions revealed that, amino acid residues residues Asn 94, Arg 133 , Tyr 137 , Ile 139 , Ala 148, Tyr 149 ,Cys 196 ,Val 197 ,and Val 198 are key residues in caspase-7, whereas residues Tyr 46 , Ala 49 , Phe 50, Leu 53 , Val 71, Leu 75, , Arg 84 , Ala 87 and Ser90 are key residues in BCL2 receptor. The results from our study are of great important to understand the molecular basis of activity difference between **11** against caspase-7 and BCL2 and for the design of more potent selective inhibitor. Prediction of computational drug like properties showed that compound **11** is safe with acceptable ADMET and druggable properties.

5. Conflict of interest

There is no conflict of interest**.**

6.Ethics

Since every study is conducted in vitro, ethics are not required.

Reference:

1. Viegas S, Ladeira C, Costa-Veiga A, Perelman J, Gajski G. Forgotten public health impacts of cancer-an overview.
2. Sung H, Ferlay J, Siegel RL, Laversanne M, Soerjomataram I, Jemal A, et al. Global Cancer Statistics 2020: GLOBOCAN Estimates of Incidence and Mortality Worldwide for 36 Cancers in 185 Countries. CA Cancer J Clin [Internet]. 2021 May 1 [cited 2023 Mar 22];71(3):209–49. Available from: https://onlinelibrary.wiley.com/doi/full/10.3322/caac.21660
3. Fadelu T, Rebbeck TR. The rising burden of cancer in low- and middle-Human Development Index countries. Cancer [Internet]. 2021 Aug 15 [cited 2023 Mar 22];127(16):2864–6. Available from: https://pubmed.ncbi.nlm.nih.gov/34086352/
4. Buolamwini JK. Novel anticancer drug discovery. Curr Opin Chem Biol [Internet]. 1999 [cited 2023 Mar 22];3(4):500–9. Available from: https://pubmed.ncbi.nlm.nih.gov/10419854/
5. Letai A, Bassik MC, Walensky LD, Sorcinelli MD, Weiler S, Korsmeyer SJ. Distinct BH3 domains either sensitize or activate mitochondrial apoptosis, serving as prototype cancer therapeutics. Cancer Cell. 2002 Sep 1;2(3):183–92.
6. Al-Abdullah ES. Synthesis and anticancer activity of some novel tetralin-6-yl-pyrazoline, 2-thioxopyrimidine, 2-oxopyridine, 2-thioxo-pyridine and 2-iminopyridine derivatives. Molecules. 2011 Apr;16(4):3410–9.
7. Zhu XP, Lin GS, Duan WG, Li QM, Li FY, Lu SZ. Synthesis and Antiproliferative Evaluation of Novel Longifolene-Derived Tetralone Derivatives Bearing 1,2,4-Triazole Moiety. Mol 2020, Vol 25, Page 986 [Internet]. 2020 Feb 22 [cited 2023 Mar 22];25(4):986. Available from: https://www.mdpi.com/1420-3049/25/4/986/htm
8. Campbell P, Thomas CM. Belinostat for the treatment of relapsed or refractory peripheral T-cell lymphoma. J Oncol Pharm Pract [Internet]. 2017 Mar 1 [cited 2023 Aug 29];23(2):143–7. Available from: https://pubmed.ncbi.nlm.nih.gov/26921086/
9. Verweij J, Sleijfer S. Pazopanib, a new therapy for metastatic soft tissue sarcoma. Expert Opin Pharmacother [Internet]. 2013 May [cited 2023 Aug 29];14(7):929–35. Available from: https://pubmed.ncbi.nlm.nih.gov/23488774/
10. WO2012175654A1 - Tetraline sulfonamide derivatives for use in the treatment of proliferative disorders - Google Patents [Internet]. [cited 2023 Mar 22]. Available from: https://patents.google.com/patent/WO2012175654A1/en
11. Mohamed HS, Haiba ME, Mohamed NA, Awad GEA, Ahmed NS. New hydronaphthalene-sulfonamide derivatives:

Synthesis, antimicrobial evaluation and QSAR study. J Mol Struct. 2021 Dec 15;1246:131108.
12. Mirzaei S, Eisvand F, Hadizadeh F, Mosaffa F, Ghasemi A, Ghodsi R. Design, synthesis and biological evaluation of novel 5,6,7-trimethoxy-N-aryl-2-styrylquinolin-4-amines as potential anticancer agents and tubulin polymerization inhibitors. Bioorg Chem. 2020 May 1;98.
13. Hasanin M, Hashem AH, El-Rashedy AA, Kamel S. Synthesis of novel heterocyclic compounds based on dialdehyde cellulose: characterization, antimicrobial, antitumor activity, molecular dynamics simulation and target identification. Cellulose. 2021 Sep 1;28(13):8355–74.
14. Cournia Z, Allen B, Sherman W. Relative Binding Free Energy Calculations in Drug Discovery: Recent Advances and Practical Considerations. Vol. 57, Journal of Chemical Information and Modeling. American Chemical Society; 2017. p. 2911–37.
15. Daina A, Michielin O, Zoete V. ILOGP: A simple, robust, and efficient description of n-octanol/water partition coefficient for drug design using the GB/SA approach. J Chem Inf Model. 2014;54(12):3284–301.
16. Ali IH, Abdel-Mohsen HT, Mounier MM, Abo-elfadl MT, El Kerdawy AM, Ghannam IAY. Design, synthesis and anticancer activity of novel 2-arylbenzimidazole/2-thiopyrimidines and 2-thioquinazolin-4(3H)-ones conjugates as targeted RAF and VEGFR-2 kinases inhibitors. Bioorg Chem [Internet]. 2022 Sep 1 [cited 2023 Aug 29];126. Available from: https://pubmed.ncbi.nlm.nih.gov/35636123/
17. Mounier MM, Shehata SH, Soliman TN. Anticancer activity of nanoencapsulated ginger in whey proteins against human tumor cell lines. Egypt Pharm J. 2020;19(2):87–96.
18. Denault JB, Salvesen GS. Human caspase-7 activity and regulation by its N-terminal peptide. J Biol Chem [Internet]. 2003 Sep 5 [cited 2023 Aug 29];278(36):34042–50. Available from: https://pubmed.ncbi.nlm.nih.gov/12824163/
19. Barbareschi M, Caffo O, Veronese S, Leek RD, Fina P, Fox S, et al. Bcl-2 and p53 expression in node-negative breast carcinoma: a study with long-term follow-up. Hum Pathol [Internet]. 1996 [cited 2023 Aug 29];27(11):1149–55. Available from: https://pubmed.ncbi.nlm.nih.gov/8912823/
20. Onur R, Semerciöz A, Orhan I, Yekeler H. The effects of melatonin and the antioxidant defence system on apoptosis regulator proteins (Bax and Bcl-2) in experimentally induced varicocele. Urol Res [Internet]. 2004 [cited 2023 Aug 29];32(3):204–8. Available from: https://pubmed.ncbi.nlm.nih.gov/15205854/
21. Diab S, Teo T, Kumarasiri M, Li P, Yu M, Lam F, et al. Discovery of 5-(2-(Phenylamino)pyrimidin-4-yl)thiazol-2(3H)-one Derivatives as Potent Mnk2 Inhibitors: Synthesis, SAR Analysis and Biological Evaluation. ChemMedChem [Internet]. 2014 May 1 [cited 2023 Aug 29];9(5):962–72. Available from: https://onlinelibrary.wiley.com/doi/full/10.1002/cmdc.201300552
22. Hardy JA, Lam J, Nguyen JT, O'Brien T, Wells JA. Discovery of an allosteric site in the caspases. Proc Natl Acad Sci U S A [Internet]. 2004 Aug 24 [cited 2022 Nov 17];101(34):12461–6. Available from: https://www.pnas.org/doi/abs/10.1073/pnas.0404781101
23. Zhou H, Chen J, Meagher JL, Yang CY, Aguilar A, Liu L, et al. Design of Bcl-2 and Bcl-xL inhibitors with subnanomolar binding affinities based upon a new scaffold. J Med Chem [Internet]. 2012 May 24 [cited 2023 Jan 24];55(10):4664–82. Available from: https://pubmed.ncbi.nlm.nih.gov/22448988/
24. Pettersen EF, Goddard TD, Huang CC, Couch GS, Greenblatt DM, Meng EC, et al. UCSF Chimera--a visualization system for exploratory research and analysis. J Comput Chem. 2004;25(13):1605–12.
25. Li H, Robertson AD, Jensen JH. Very fast empirical prediction and rationalization of protein pKa values. Proteins [Internet]. 2005 Dec 1 [cited 2022 Sep 11];61(4):704–21. Available from: https://pubmed.ncbi.nlm.nih.gov/16231289/
26. BETHANY HALFORD. Reflections On ChemDraw. Chem Eng News Arch. 2014 Aug 18;92(33):26–7.
27. Hospital A, Goñi JR, Orozco M, Gelpí JL. Molecular dynamics simulations: advances and applications. Adv Appl Bioinform Chem [Internet]. 2015 Nov [cited 2017 Jun 14];8:37–47. Available from: https://www.dovepress.com/molecular-dynamics-simulations-advances-and-applications-peer-reviewed-article-AABC
28. Lee TS, Cerutti DS, Mermelstein D, Lin C, Legrand S, Giese TJ, et al. GPU-Accelerated Molecular Dynamics and Free Energy Methods in Amber18: Performance Enhancements and New Features. J Chem Inf Model. 2018 Oct 22;58(10):2043–50.
29. Wang J, Wang W, Kollman PA, Case DA. Automatic atom type and bond type perception in molecular mechanical

calculations. J Mol Graph Model. 2006;25(2):247–60.
30. Berendsen HJC, Postma JPM, van Gunsteren WF, DiNola A, Haak JR. Molecular dynamics with coupling to an external bath. J Chem Phys [Internet]. 1984 Oct 15 [cited 2017 Jun 21];81(8):3684–90. Available from: http://aip.scitation.org/doi/10.1063/1.448118
31. Roe DR, Cheatham TE. PTRAJ and CPPTRAJ: Software for Processing and Analysis of Molecular Dynamics Trajectory Data. J Chem Theory Comput [Internet]. 2013 Jul 9 [cited 2018 Jul 12];9(7):3084–95. Available from: http://pubs.acs.org/doi/10.1021/ct400341p
32. Seifert E. OriginPro 9.1: Scientific data analysis and graphing software - Software review. J Chem Inf Model. 2014;54(5):1552–1552.
33. Pettersen EF, Goddard TD, Huang CC, Couch GS, Greenblatt DM, Meng EC, et al. UCSF Chimera--a visualization system for exploratory research and analysis. J Comput Chem [Internet]. 2004 Oct [cited 2017 Jun 13];25(13):1605–12. Available from: http://doi.wiley.com/10.1002/jcc.20084
34. Kollman PA, Massova I, Reyes C, Kuhn B, Huo S, Chong L, et al. Calculating structures and free energies of complex molecules: combining molecular mechanics and continuum models. Acc Chem Res. 2000 Dec;33(12):889–97.
35. Ylilauri M, Pentikäinen OT. MMGBSA as a tool to understand the binding affinities of filamin-peptide interactions. J Chem Inf Model [Internet]. 2013 Oct 28 [cited 2018 Feb 23];53(10):2626–33. Available from: http://pubs.acs.org/doi/10.1021/ci4002475
36. M. J, Archontis G. MM-GB(PB)SA Calculations of Protein-Ligand Binding Free Energies. In: Molecular Dynamics - Studies of Synthetic and Biological Macromolecules [Internet]. InTech; 2012 [cited 2018 Feb 28]. Available from: http://www.intechopen.com/books/molecular-dynamics-studies-of-synthetic-and-biological-macromolecules/mm-gb-pb-sa-calculations-of-protein-ligand-binding-free-energies
37. Hou T, Wang J, Li Y, Wang W. Assessing the performance of the MM/PBSA and MM/GBSA methods. 1. The accuracy of binding free energy calculations based on molecular dynamics simulations. J Chem Inf Model. 2011;51(1):69–82.
38. Greenidge PA, Kramer C, Mozziconacci JC, Wolf RM. MM/GBSA binding energy prediction on the PDBbind data set: Successes, failures, and directions for further improvement. J Chem Inf Model. 2013;53(1):201–9.
39. Sitkoff D, Sharp KA, Honig B. Accurate calculation of hydration free energies using macroscopic solvent models. J Phys Chem. 1994;98(7):1978–88.
1. Viegas S, Ladeira C, Costa-Veiga A, Perelman J, Gajski G. Forgotten public health impacts of cancer-an overview.
2. Sung H, Ferlay J, Siegel RL, Laversanne M, Soerjomataram I, Jemal A, et al. Global Cancer Statistics 2020: GLOBOCAN Estimates of Incidence and Mortality Worldwide for 36 Cancers in 185 Countries. CA Cancer J Clin [Internet]. 2021 May 1 [cited 2023 Mar 22];71(3):209–49. Available from: https://onlinelibrary.wiley.com/doi/full/10.3322/caac.21660
3. Fadelu T, Rebbeck TR. The rising burden of cancer in low- and middle-Human Development Index countries. Cancer [Internet]. 2021 Aug 15 [cited 2023 Mar 22];127(16):2864–6. Available from: https://pubmed.ncbi.nlm.nih.gov/34086352/
4. Buolamwini JK. Novel anticancer drug discovery. Curr Opin Chem Biol [Internet]. 1999 [cited 2023 Mar 22];3(4):500–9. Available from: https://pubmed.ncbi.nlm.nih.gov/10419854/
5. Letai A, Bassik MC, Walensky LD, Sorcinelli MD, Weiler S, Korsmeyer SJ. Distinct BH3 domains either sensitize or activate mitochondrial apoptosis, serving as prototype cancer therapeutics. Cancer Cell. 2002 Sep 1;2(3):183–92.
6. Al-Abdullah ES. Synthesis and anticancer activity of some novel tetralin-6-yl-pyrazoline, 2-thioxopyrimidine, 2-oxopyridine, 2-thioxo-pyridine and 2-iminopyridine derivatives. Molecules. 2011 Apr;16(4):3410–9.
7. Zhu XP, Lin GS, Duan WG, Li QM, Li FY, Lu SZ. Synthesis and Antiproliferative Evaluation of Novel Longifolene-Derived Tetralone Derivatives Bearing 1,2,4-Triazole Moiety. Mol 2020, Vol 25, Page 986 [Internet]. 2020 Feb 22 [cited 2023 Mar 22];25(4):986. Available from: https://www.mdpi.com/1420-3049/25/4/986/htm
8. Campbell P, Thomas CM. Belinostat for the treatment of relapsed or refractory peripheral T-cell lymphoma. J Oncol Pharm Pract [Internet]. 2017 Mar 1 [cited 2023 Aug 29];23(2):143–7. Available from: https://pubmed.ncbi.nlm.nih.gov/26921086/
9. Verweij J, Sleijfer S. Pazopanib, a new therapy for metastatic soft tissue sarcoma. Expert Opin Pharmacother [Internet]. 2013 May [cited 2023 Aug 29];14(7):929–35.

Available from: https://pubmed.ncbi.nlm.nih.gov/23488774/
10. WO2012175654A1 - Tetraline sulfonamide derivatives for use in the treatment of proliferative disorders - Google Patents [Internet]. [cited 2023 Mar 22]. Available from: https://patents.google.com/patent/WO2012175654A1/en
11. Mohamed HS, Haiba ME, Mohamed NA, Awad GEA, Ahmed NS. New hydronaphthalene-sulfonamide derivatives: Synthesis, antimicrobial evaluation and QSAR study. J Mol Struct. 2021 Dec 15;1246:131108.
12. Mirzaei S, Eisvand F, Hadizadeh F, Mosaffa F, Ghasemi A, Ghodsi R. Design, synthesis and biological evaluation of novel 5,6,7-trimethoxy-N-aryl-2-styrylquinolin-4-amines as potential anticancer agents and tubulin polymerization inhibitors. Bioorg Chem. 2020 May 1;98.
13. Hasanin M, Hashem AH, El-Rashedy AA, Kamel S. Synthesis of novel heterocyclic compounds based on dialdehyde cellulose: characterization, antimicrobial, antitumor activity, molecular dynamics simulation and target identification. Cellulose. 2021 Sep 1;28(13):8355–74.
14. Cournia Z, Allen B, Sherman W. Relative Binding Free Energy Calculations in Drug Discovery: Recent Advances and Practical Considerations. Vol. 57, Journal of Chemical Information and Modeling. American Chemical Society; 2017. p. 2911–37.
15. Daina A, Michielin O, Zoete V. ILOGP: A simple, robust, and efficient description of n-octanol/water partition coefficient for drug design using the GB/SA approach. J Chem Inf Model. 2014;54(12):3284–301.
16. Ali IH, Abdel-Mohsen HT, Mounier MM, Abo-elfadl MT, El Kerdawy AM, Ghannam IAY. Design, synthesis and anticancer activity of novel 2-arylbenzimidazole/2-thiopyrimidines and 2-thioquinazolin-4(3H)-ones conjugates as targeted RAF and VEGFR-2 kinases inhibitors. Bioorg Chem [Internet]. 2022 Sep 1 [cited 2023 Aug 29];126. Available from: https://pubmed.ncbi.nlm.nih.gov/35636123/
17. Mounier MM, Shehata SH, Soliman TN. Anticancer activity of nanoencapsulated ginger in whey proteins against human tumor cell lines. Egypt Pharm J. 2020;19(2):87–96.
18. Denault JB, Salvesen GS. Human caspase-7 activity and regulation by its N-terminal peptide. J Biol Chem [Internet]. 2003 Sep 5 [cited 2023 Aug 29];278(36):34042–50. Available from: https://pubmed.ncbi.nlm.nih.gov/12824163/
19. Barbareschi M, Caffo O, Veronese S, Leek RD, Fina P, Fox S, et al. Bcl-2 and p53 expression in node-negative breast carcinoma: a study with long-term follow-up. Hum Pathol [Internet]. 1996 [cited 2023 Aug 29];27(11):1149–55. Available from: https://pubmed.ncbi.nlm.nih.gov/8912823/
20. Onur R, Semerciöz A, Orhan I, Yekeler H. The effects of melatonin and the antioxidant defence system on apoptosis regulator proteins (Bax and Bcl-2) in experimentally induced varicocele. Urol Res [Internet]. 2004 [cited 2023 Aug 29];32(3):204–8. Available from: https://pubmed.ncbi.nlm.nih.gov/15205854/
21. Diab S, Teo T, Kumarasiri M, Li P, Yu M, Lam F, et al. Discovery of 5-(2-(Phenylamino)pyrimidin-4-yl)thiazol-2(3H)-one Derivatives as Potent Mnk2 Inhibitors: Synthesis, SAR Analysis and Biological Evaluation. ChemMedChem [Internet]. 2014 May 1 [cited 2023 Aug 29];9(5):962–72. Available from: https://onlinelibrary.wiley.com/doi/full/10.1002/cmdc.201300552
22. Hardy JA, Lam J, Nguyen JT, O'Brien T, Wells JA. Discovery of an allosteric site in the caspases. Proc Natl Acad Sci U S A [Internet]. 2004 Aug 24 [cited 2022 Nov 17];101(34):12461–6. Available from: https://www.pnas.org/doi/abs/10.1073/pnas.0404781101
23. Zhou H, Chen J, Meagher JL, Yang CY, Aguilar A, Liu L, et al. Design of Bcl-2 and Bcl-xL inhibitors with subnanomolar binding affinities based upon a new scaffold. J Med Chem [Internet]. 2012 May 24 [cited 2023 Jan 24];55(10):4664–82. Available from: https://pubmed.ncbi.nlm.nih.gov/22448988/
24. Pettersen EF, Goddard TD, Huang CC, Couch GS, Greenblatt DM, Meng EC, et al. UCSF Chimera--a visualization system for exploratory research and analysis. J Comput Chem. 2004;25(13):1605–12.
25. Li H, Robertson AD, Jensen JH. Very fast empirical prediction and rationalization of protein pKa values. Proteins [Internet]. 2005 Dec 1 [cited 2022 Sep 11];61(4):704–21. Available from: https://pubmed.ncbi.nlm.nih.gov/16231289/
26. BETHANY HALFORD. Reflections On ChemDraw. Chem Eng News Arch. 2014 Aug 18;92(33):26–7.
27. Hospital A, Goñi JR, Orozco M, Gelpí JL. Molecular dynamics simulations: advances and applications. Adv Appl Bioinform Chem [Internet]. 2015 Nov [cited 2017 Jun 14];8:37–47. Available from:

https://www.dovepress.com/molecular-dynamics-simulations-advances-and-applications-peer-reviewed-article-AABC
28. Lee TS, Cerutti DS, Mermelstein D, Lin C, Legrand S, Giese TJ, et al. GPU-Accelerated Molecular Dynamics and Free Energy Methods in Amber18: Performance Enhancements and New Features. J Chem Inf Model. 2018 Oct 22;58(10):2043–50.
29. Wang J, Wang W, Kollman PA, Case DA. Automatic atom type and bond type perception in molecular mechanical calculations. J Mol Graph Model. 2006;25(2):247–60.
30. Berendsen HJC, Postma JPM, van Gunsteren WF, DiNola A, Haak JR. Molecular dynamics with coupling to an external bath. J Chem Phys [Internet]. 1984 Oct 15 [cited 2017 Jun 21];81(8):3684–90. Available from: http://aip.scitation.org/doi/10.1063/1.448118
31. Roe DR, Cheatham TE. PTRAJ and CPPTRAJ: Software for Processing and Analysis of Molecular Dynamics Trajectory Data. J Chem Theory Comput [Internet]. 2013 Jul 9 [cited 2018 Jul 12];9(7):3084–95. Available from: http://pubs.acs.org/doi/10.1021/ct400341p
32. Seifert E. OriginPro 9.1: Scientific data analysis and graphing software - Software review. J Chem Inf Model. 2014;54(5):1552–1552.
33. Pettersen EF, Goddard TD, Huang CC, Couch GS, Greenblatt DM, Meng EC, et al. UCSF Chimera--a visualization system for exploratory research and analysis. J Comput Chem [Internet]. 2004 Oct [cited 2017 Jun 13];25(13):1605–12. Available from: http://doi.wiley.com/10.1002/jcc.20084
34. Kollman PA, Massova I, Reyes C, Kuhn B, Huo S, Chong L, et al. Calculating structures and free energies of complex molecules: combining molecular mechanics and continuum models. Acc Chem Res. 2000 Dec;33(12):889–97.
35. Ylilauri M, Pentikäinen OT. MMGBSA as a tool to understand the binding affinities of filamin-peptide interactions. J Chem Inf Model [Internet]. 2013 Oct 28 [cited 2018 Feb 23];53(10):2626–33. Available from: http://pubs.acs.org/doi/10.1021/ci4002475
36. M. J, Archontis G. MM-GB(PB)SA Calculations of Protein-Ligand Binding Free Energies. In: Molecular Dynamics - Studies of Synthetic and Biological Macromolecules [Internet]. InTech; 2012 [cited 2018 Feb 28]. Available from: http://www.intechopen.com/books/molecular-dynamics-studies-of-synthetic-and-biological-macromolecules/mm-gb-pb-sa-calculations-of-protein-ligand-binding-free-energies
37. Hou T, Wang J, Li Y, Wang W. Assessing the performance of the MM/PBSA and MM/GBSA methods. 1. The accuracy of binding free energy calculations based on molecular dynamics simulations. J Chem Inf Model. 2011;51(1):69–82.
38. Greenidge PA, Kramer C, Mozziconacci JC, Wolf RM. MM/GBSA binding energy prediction on the PDBbind data set: Successes, failures, and directions for further improvement. J Chem Inf Model. 2013;53(1):201–9.
39. Sitkoff D, Sharp KA, Honig B. Accurate calculation of hydration free energies using macroscopic solvent models. J Phys Chem. 1994;98(7):1978–88.